Master in Advanced Telecommunications Technologies

3D BEAMSTEERING LOW COMPLEXITY RECONFIGURABLE MULTILEVEL ANTENNA

Ivan Zhou

Supervised by Dr. Lluís Jofre

Presented on date 30^{th} $January$ 2020

Registered at

Escola Tècnica Superior d'Enginyeria de Telecomunicació de Barcelona

CONTENTS

1. Introduction 1

2. Summary 3

3. Overview of Beam Steering techniques 4
  3.1 Mechanical 4
  3.2 Beamforming 4
    3.2.1 RF/Analog 4
    3.2.2 Digital 5
    3.2.3 Hybrid 6
  3.3 Reflectarrays 6
  3.4 Integrated Lens Antennas 6
  3.5 Switched Beam Antennas 7
  3.6 Metamaterials 7
  3.7 Conclusions 8

4. Principle of Reconfigurable antennas 9
  4.1 Types of Reconfigurable antennas 9
    4.1.1 Frequency reconfigurability 9
    4.2.1 Polarization reconfigurability 10
    4.2.2 Pattern reconfigurability 10

5. 3D Beam-Steering Reconfigurable Antenna 14
  5.1 Design of the antenna 14
    5.1.1 Principal Geometry of the antenna 15
    5.1.1 Working principle 17
    5.1.2 Experimental results 20
  5.2 Improved Radiation Pattern design 23
  5.3 Dual Polarized 3D Beam-Steering antenna 26

6. Conclusions 28

7. References 29

LIST OF ACRONYMS

NR	New Radio
FR	Frequency Range
RPL	Reconfigurable Parasitic Layer
PL	Parasitic Layer
RA	Reconfigurable antenna
ESPAR	Electronically steerable reconfigurable parasitic array
MEMs	Microelectromechanical systems
RF	Radio Frequency
PA	Phased Arrays
BS	Beam-Steering
ILA	Integrated Lens Antenna
LOS	Line of Sight
DP	Double Polarization
FBW	Fractional Bandwidth

1. Introduction

Beamforming, in its many variants, is a key spatial processing technique to improve user throughput, system capacity, system coverage as well as reducing interference [1]. Simple architectures enabling beamforming either in predefined or arbitrary directions are very desirable for the Fifth Generation of Mobile Communications (5G) to boost power efficiency. Furthermore, it is expected that the number of 5G mobile subscribers grows from 5 million in 2019 to nearly 600 million by 2023, increasing traffic, connections density, and latency which will increase the demand of capacity to the network. Therefore, a broadband intelligent antenna must be at the basis to provide reliable data service.

Two appealing cost-efficient and low-complexity alternatives to conventional beamformers, which are generally based on phase-shifters or line-delays matrices, are the Electronically Steerable Parasitic Array (ESPAR) and the Parasitic Layer (PL) see Fig. 1, whose principles are on the basis of the antenna presented in this work.

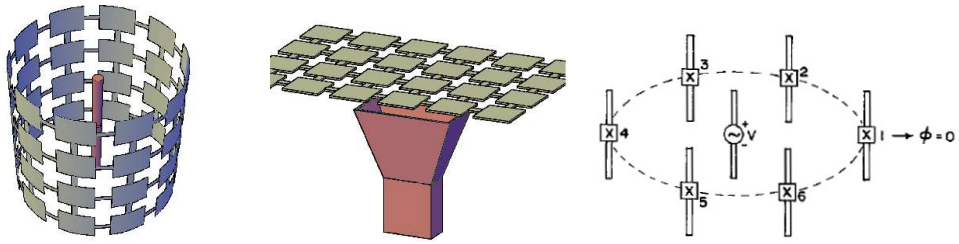

Fig. 1 Dipole surrounded by a cylindric pixelated reconfigurable PL in the left and ESPAR concept in the right.

On the one hand, ESPAR beamformers, originally proposed in [2], consist of a driven antenna element surrounded by N reactively loaded parasitic elements. With this arrangement, beamsteering as well as superdirectivity can be achieved by changing the reactive impedance of each parasitic element. Later works based on similar ideas and coining the ESPAR term can be found in [3] and [4].

On a similar line of thought, the Reconfigurable PL concept [5] is an approach to provide added functionalities to a basic antenna, e.g. the ability to adjust dynamically the match frequency, polarization and radiation properties. The switches used in the PL can be either PIN diodes [6, 7], microelectromechanical system (MEMs) switches [8] or varactor diodes [9]. RAs using PIN diodes are widespread due to their fast switching speed and low cost compared to MEMs, and higher energy efficiency and reduced losses when contrasted with varactors.

One of the successful applications of the PL concept is to add beam-steering capabilities to microstrip patch antennas. Similarly, large and medium complexity PL [10, 11] have been used to add polarization shifting to single-port antennas, although this usually comes at the expense of using a larger amount of switching elements. Cost and reliability criteria have led to recent modifications of the PL concept, aiming to reduce the number of switches and thus the complexity of design. three examples of simplified PL are [12-14]. The design outlined in [14] despite using a very reduced number of switches, is bandwidth limited.

In contrast to the traditional ESPAR, in this work the parasitic elements are arranged in a new multilevel geometry and are switched ON/OFF instead of acting as loads of variable value. In

comparison to the antennas presented in the literature, the novelty of the proposed antenna lies in its capability to steer its beam to up to nine different angular directions based on a novel geometry as mentioned before using only four PIN diodes as switches, leading the design to the most simple one in terms of number of switches.

2. Summary

In the first part of this thesis we will review some basic concepts of the main beam-steering (BS) techniques used in the literature. By seeing each one of them we will get better insights about its advantages and limitations. One of the most attractive BS techniques are the ones implemented by Reconfigurable Antennas (RAs), because they offer a low cost and compact way to steer the beam when compared to conventional techniques like phased arrays and mechanical steering to mention some. We will review some successful RA designs showing its main working principles in pattern reconfigurability.

The second part consists in the design of a novel RA for beam-steering. We will present a rigorous mathematical development of the theory that explains the antenna's working principle, which is in fact very rarely seen nowadays in antenna design papers. We will eventually prove the theoretical concept with the simulations and measurement results from a manufactured prototype of the antenna.

Finally, we will show two improved designs of the antenna. One by using two more switches we enhance the directivity and steered angles of the different beam patterns, and double de number of operation modes. And the other one by employing the capability of double polarization we succeed to steer the beam into nine different directions for both horizontal and vertical polarizations independently.

3. Beam-Steering techniques

Beam-Steering (BS) is about changing the direction of the antenna's radiation pattern main lobe. By focusing it to the desired direction, we can reduce interference, increase gain and radiation efficiency. For radar based applications for example, it is an indispensable technology because tracking of the target is required. There are many ways to achieve BS, in this chapter we present the main techniques that we can find in the literature, each one with its advantages and inconveniences.

3.1 Mechanical steering

This involves manually turning the antenna to face the direction of interest, see Fig. 3.1. Mechanical steering is often performed by means of electric motors. Recently, MEMS devices have been used to implement mechanical steering [15], they offer improved speed of scanning compared to manually steered arrays as well as low losses to the system. Mechanical steering is highly effective since it maintains the gain of the antenna and offers flexibility in the steering range of the antenna. However it becomes undesirable and difficult when we consider factors such as antenna size, weight, and weather conditions.

Fig. 3.1 Rotating marine Radar

Also its use is limited to static or very slow changing environments due to the limitation in steering speed. Furthermore, rotating mechanisms are prone to mechanical failure due to fatigue and wearing of moving parts. The solutions for these problems led to electronic ways of steering beams.

3.2 Beamforming

The term beamforming [16] refers to the process of combining signals from an array of elements to form a highly directional beam of radiation to the desired direction. Beamforming techniques can be subclassified as RF/analogue, digital, or hybrid beamforming.

3.2.1 RF/analogue beamforming

RF/analogue beamforming, also known as Phased arrays (PA) have been the conventional way of steering beams electronically to different directions within the range of the element pattern. By changing the phases of each element in the array with phase shifters, the combined beam of the array is steered. It has the advantage of high directivity, multiple beamforming (one at a time in different directions), fast scanning when compared to mechanical steering due to its electronic circuitry, and spatial filtering.

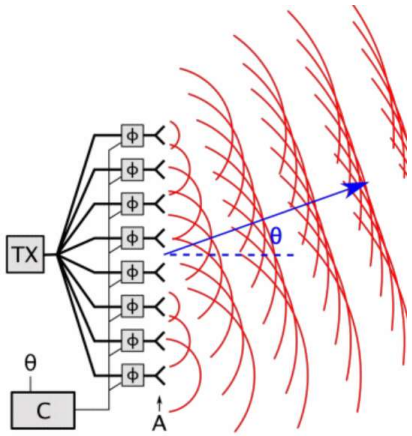

Fig. 3.2 Phased array antenna for beam steering

Analogue phase shifters are built with varactor diodes and offer continuous phase shift by controlling the voltage of the varactor diodes. This control voltage is highly influenced by noise and incurs heavy losses to the device. For this reason, digital phase shifters have received much attention due to their immunity to the noise present on voltage control lines. There are several techniques used to implement digital phase shifters, some of which are switched-line [17], loaded-line [18], reflection-type [19], and vector modulator technique phase shifters [20].

3.2.2 Digital beamforming

In digital beamforming [21], the signals from each antenna element are sampled by an ADC, down converted to have the baseband signal and then is split into different channels by using channelisers. The resulting channels are then fed into a beamformer. The beamformer applies steering and correction coefficients to each channel before summing the channels to produce a radiated beam.

Digital beamforming can be performed over wide bandwidths due to its ability to split the signals into various channels. Two main approaches for wideband beamforming are based on time-domain processing and frequency domain processing [22]. Time domain processing is performed using tapped delay line filters, the length of the lines depend on the bandwidth of signals. Frequency-domain processing is performed by using a Fast Fourier transform to convert the wideband signal into frequency domain. Each converted signal is then processed by a narrowba-

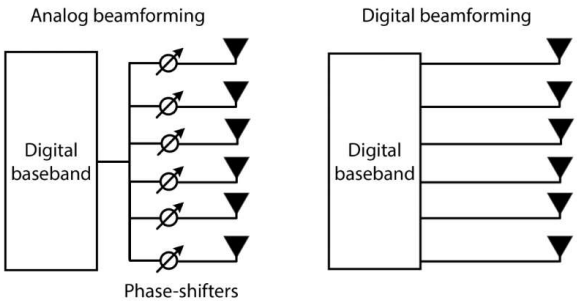

Fig. 3.3 Comparison between analog and digital beamforming

nd processor domain. These approaches can produce beamforming without bandwidth phase deviation which enables a beam to steer uniformly over its operating bandwidth. However, it has high power requirement and large cost.

3.2.3 Hybrid beamforming

Recently, interest is growing in a hybrid of analogue and digital beamforming that is intended to reduce the complexity of digital beamforming and improve the performance of analogue beamforming. The RF/analogue beamforming section controls the phase of the signal at each element while the digital beamforming section applies baseband signal processing to enhance the performance of the multiple data channels. Recent work in the area of RF beamforming have concentrated on reducing the losses associated with phase shifters. Currently, the major research interests in digital beamforming concentrate on algorithms to improve the computational time and signal tracking.

3.3 Reflectarray

A reflectarray [23] is formed from the combination of a reflector and an array antenna, see Fig. 3.3. The aim, in combining the two technologies, is to use the strengths of each to maximum advantage.

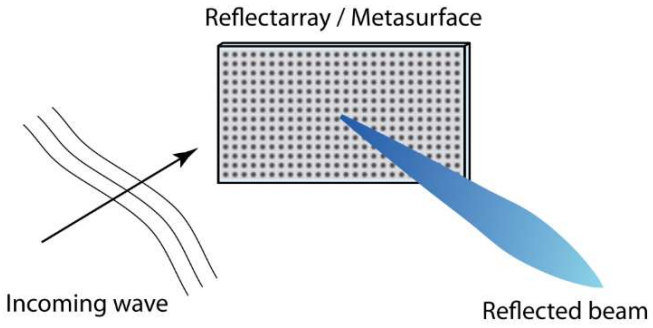

Fig. 3.3 Reflectarray working principle

The array is designed to redirect the incident waves by applying predefined phases to different sections of the array. The predefined phases are either set actively, by using phase shifters for all the elements of the array or passively, by the shape and size of each one of them. It has the advantage of generating multiple beams which can be used for point-to-multipoint applications by applying different phase shifts to sections of the array. However, due to the presence of phase shifters, reflectarray also suffers from losses induced by phase shifters. It also has the limitation of predefined beams as with phased arrays since it has phase shifters and does not offer continuous beam steering. With increasing number of elements, the complexity and cost of reflectarray increases.

3.4 Integrated lens antennas (ILAs)

The concept of integrating a lens over a planar radiating element was developed by Rutledge [24] and has seen much improvement since then. Generally, an ILA consists of an elliptical or quasi elliptical dielectric lens and an array of switched feed elements integrated on the lens back focal plane. The lens collimating surface produces a focused beam in the direction predetermined by the position of a corresponding feed element relatively to the lens central axis.

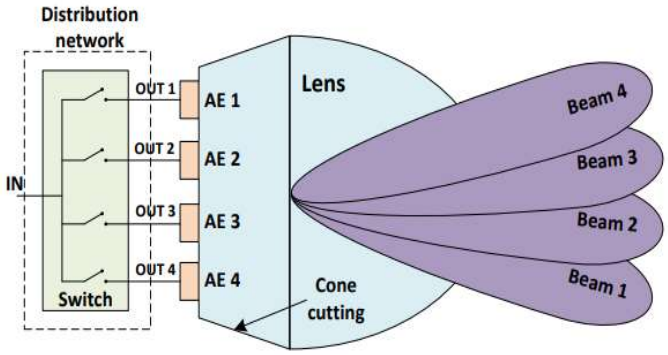

Fig. 3.4 Example of ILA

The ILA achieves a highly directional beam using fewer elements when compared with a phased array antenna. ILAs also employ RF switches instead of phase shifters which have lower losses, offer simplicity and lower cost when compared to phase shifters.

3.5 Switched beam antennas

This is a technique where antenna elements are arranged to cover an angle range of interest. Each element covers a section of the total range and is turned on when there is a need to radiate in that particular direction. This arrangement is a bit similar to that of ILAs without the lens. However, this solution is inefficient due to high cost and redundancy because only one element of the arrangement is used to steer the beam in the desired direction. This redundancy is present for all operating cases except point to multipoint transmission, where more than one antenna element can be turned on simultaneously. However this scenario may lead to problems due to high mutual coupling between the antenna elements. This can become a challenge to resolve. Also, if the receiving antenna falls in the region between the sectors (the boundary between consecutive antennas), connectivity cannot be guaranteed.

3.6 Metamaterial Antennas

The concept of Metameterials was proposed by Veselago in 1968 [25]. They are man-made structures that are designed to exhibit electromagnetic properties that cannot be achieved from natural occurring structures. Metamaterial have become attractive as their effective permittivity and permeability can be tuned to positive or negative values. With this property, its refractive index can be tuned using active elements such as diodes and transistors. This results in active metamaterials which have found wide use in steering an antenna's radiation pattern without the use of complex designs of feeding network and phase shifters. When used in antennas, metamaterials are realised by printing sub-wavelength metallic cells periodically on a substrate [26] and placed on a layer above the radiating element and used as a frequency selective surface (FSS). To achieve steering, the cells are loaded with varactors. By tuning each cell to different capacitance, the permeability and permittivity of the material changes hence changing the refractive index of the material.

Lastly, most authors claim that using metamaterials for steering is less complex when compared to phased array antennas, however integrating the active devices and biasing circuits into each cell of each layer and the multiple layers seems to be quite complex to achieve and a lot more difficult to fabricate.

3.7 Conclusions

The increasing demand of high data rate requires broadband antennas to satisfy that, for that reason many antennas using metamaterials and reflectarrays may not be able to support high data rates.

Regarding steering resolution, except for mechanical steering, retrodirective arrays and digital beamforming, the rest of the steering techniques suffer from limited steering resolution. Fine steering resolution may be required, specially at millimetre frequencies.

Technique	Complexity	Speed	BW	Coverage	Size	Cost
Mechanical	Low	Slow	High	High	Large	Low
Switched beams	Low	High	High	Medium	Large	Medium
Metamaterials	Moderate	-	Low	Medium	-	Low
Beamforming	High	High	-	High	Medium	High
Reflectarray	Moderate	-	Low	High	Large	High
ILAs	High	-	-	Medium	Medium	Medium/Low
RA	Low	High	High	Medium/High	Freq. Dep	Low

Table 3.1 Comparison of complexity, speed, bandwidth, coverage, size and cost among the presented techniques.

Phase shifters increases drastically the cost and complexity of the antenna when the number of elements is increased, as well as losses due to their insertion loss. Two of the discussed techniques that needs the use of phase shifters are analog, hybrid beamforming and reflectarrays.

For 5G communication purposes, beamforming in its many variants, ILAs and RA are the three best candidates. As they offer high bandwidth, high steering speed, decent coverage in a very compact and reduced size. While RAs avoids the use of phase shifters by using parasitic elements for beam-steering, beamforming can provide finer steering resolution at the cost of more expensive and complex design. Among them, the selection will depend on the application, for base stations, mobile phones or connected vehicles.

Details for the RA case will be given in chapter 4, as it is directly related with the main scope of this thesis.

4. Reconfigurable Antennas

A reconfigurable antenna (RA) is an antenna that incorporates an internal mechanism to redistribute the RF-currents over its surface and produce reversible modifications over the antenna impedance and/or radiation properties. Under this definition it is required that the reconfiguration mechanism interacts directly with the antenna radiation mechanism.

One of the most successful ways to achieve reconfigurability is by using the PL concept. PL for BS purposes is similar to ESPAR concept original from Harrington [2] as discussed in the introduction but in a much more reduced size and compact form. It also offers richer capabilities as frequency, polarization and beam-steering can be reconfigured at the same time [5] while ESPAR can only achieve pattern reconfiguration.

There are many reconfiguration mechanisms such as MEMs [8], varactor diodes [9] and PIN diodes [6,7] to mention some of them, but PIN diodes offer higher switching speed compared to MEMs making it a better candidate for fast adapting systems, and it is more energy efficient than varactor diodes as they don't need a constant voltage supply (ON/OFF state).

The most significant impulse to RAs has been undoubtedly the explosive growth of wireless personal communications devices that started in the 1990s with the deployment of GSM cellular networks. Personal wireless devices brought new requirements in terms of compactness and mobility. In the context where compactness, multi-functionality and superior performance are the main requirements, reconfigurable antennas stand out as promising approach for future wireless systems.

4.1 Types of antenna Reconfigurability

RAs can be classified according to the antenna parameter that is intentionally tuned. Following this criterion RAs are divided in three groups: frequency, radiation pattern and polarization reconfigurable antennas.

4.1.1 Frequency RA

Frequency reconfigurability can be used also to reject out-band interferences. This is accomplished by synthesizing frequency responses with a band notch (high rejection coefficient) at the interference frequency while keeping a low rejection coefficient at the signal frequency as seen Fig. 4.1. A well-known problem of portable wireless devices is that the antenna matching can be compromised due to the effect of surrounding artefacts, specially important are close-body and hand effects. A reconfigurable antenna can monitor periodically the rejection

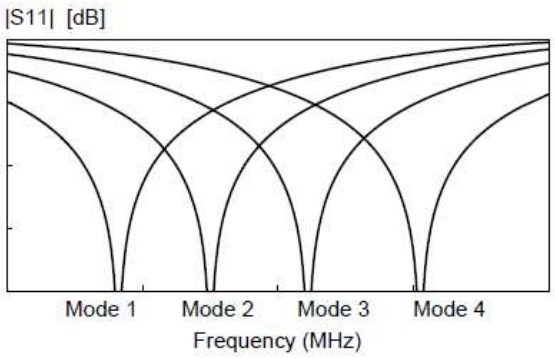

Fig. 4.1 Frequency reconfigurability

coefficient and optimize the antenna response to compensate near-body effects [27]. Finally, one of the applications recently capturing a lot of attention and where reconfigurable antennas play a key role is cognitive radio (CR). Cognitive radio transceivers sense the spectrum usage and the channel characteristics to dynamically select the operating frequency band according to specific performance metrics.

4.1.2 Polarization RA

Polarization reconfigurable antennas are typically exploited to reduce polarization mismatch losses in portable devices. The variable orientation of portable devices can degrade transmission performance if the polarization of the transmitter and receiver are not aligned. In these cases, the use of self-orientable antennas is recommended, especially in linearly polarized systems under Line of Sight (LOS) conditions [28]. Under these conditions, a polarization reconfigurable antenna switching between two orthogonal polarizations can also be used to provide a double transmission channel suitable for frequency reuse. If LOS conditions do not apply, the communications channel typically presents a high uncorrelation between horizontal and vertical polarizations. In this case, polarization reconfigurability can be used as a polarization diversity system or as a way to enhance the performance of a communication system.

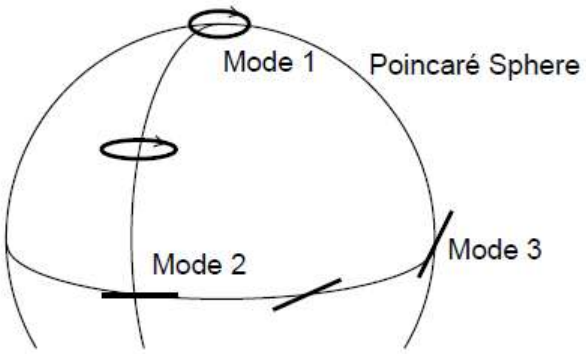

Fig. 4.2 Polarization reconfigurability modes

4.1.3 Radiation pattern RA

The most classical application is Beam-Steering as described in last chapter. Although it is known that frequency, polarization and beam-steering can be reconfigured in a single antenna realization [5] using the PL concept, it usually comes at the expense of using a large number of diodes (typically ~ 100) which reduces the radiation efficiency and reliability of the antenna. Energy and cost efficient criteria lead to actual researchers to design low complexity antennas by using a reduced number of switches. In this subsection we present some recent successful low complexity RA designs.

The first one is from Towfiq M. A. [12], see Fig. 4.4. By using an aperture coupled microstrip patch antenna and a pixelated PL in the top acting as a partial reflective surface (PRS), it is thus possible to enhance the gain of the steered beams, up to 9dB providing a broad range of operation (200MHz) at 5GHz.

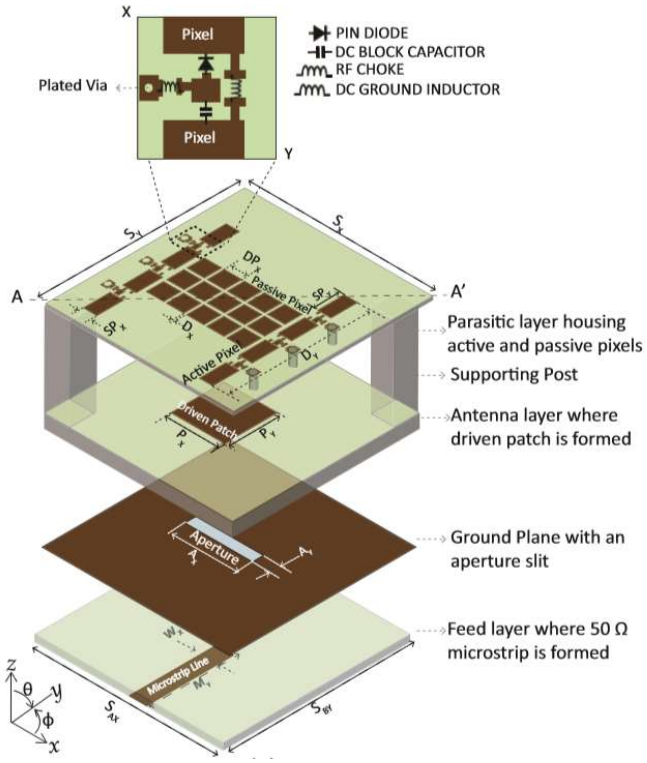

Fig. 4.4 Antenna configuration from Towfiq, M. A.

The steering mechanism relies on the pixelated strips from the two sides of the antenna. The effective electrical length of these metallic strips can be changed by switching on or off the 3 PIN diodes that interconnects them, behaving as either reflector or director (Yagi-Uda) and thus steering the beam into nine different directions.

In [7] , the design adds complexity to the previous one. Instead of using the PL as a PRS, it is used directly to reconfigure the pattern, similarly to D. Rodrigo and Ll. Jofre at [5,11]. Twelve switches are implemented in order to steer the beam up to nine different directions. The optimal configuration of the switches is achieved by using a genetic algorithm [29] which consists in evaluating a fitness function involving the input reflection coefficient and the steering angle.

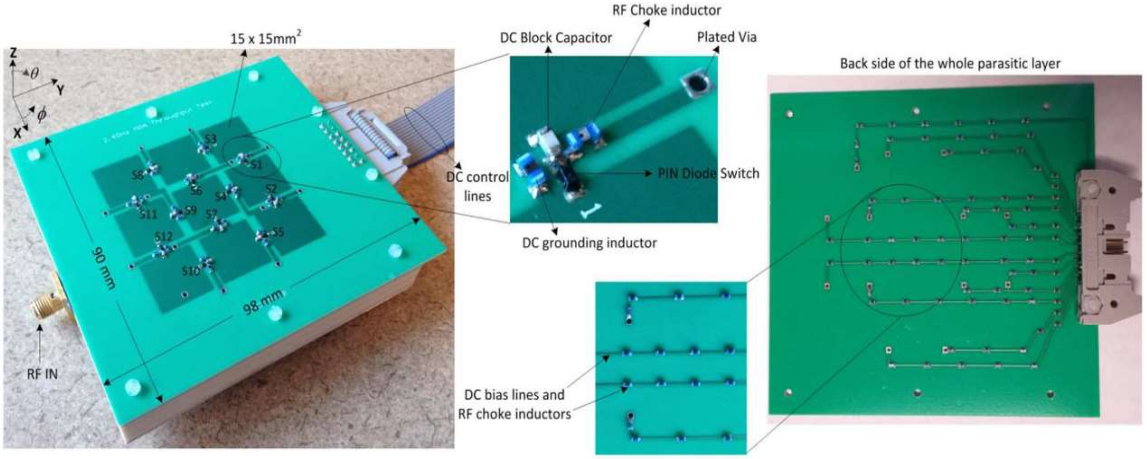

Fig. 4.5 Antenna configuration from Li, Z.

Next we have a pixelated printed monopole antenna from D. Rodrigo [11] back in 2012 designed here in the UPC facilities, see Fig 4.6.

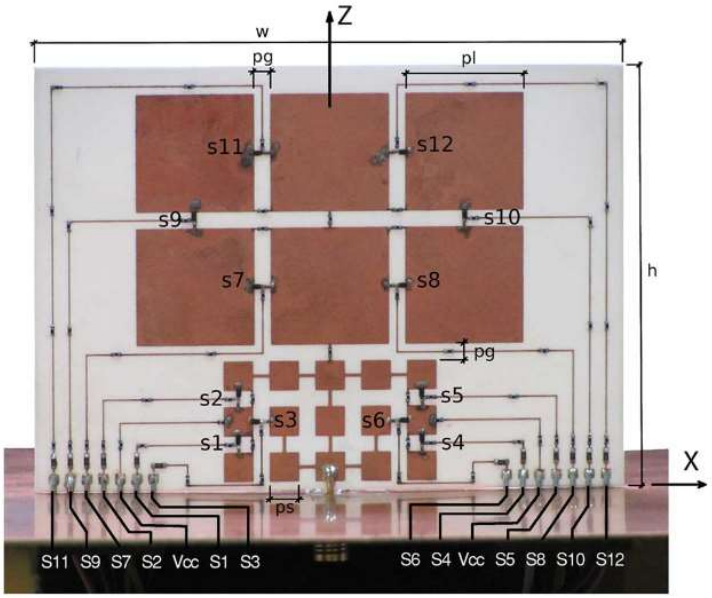

Fig. 4.6 Pixelated monopole patch antenna from D. Rodrigo

More than 30 modes of operation and 5 different frequency bands were achieved by using also 12 PIN diodes as switches. The optimal active switches combination is also found by using genetic algorithm already stated for the previous antenna.

More simple antennas can be found for example in [14] , where only four switches are implemented in order to steer the beam into 9 different directions. It is also based in the Yagi-Uda antenna like [12] by Towfiq M., there are four circular parasitic patch antennas that surrounds an active circular patch located at the centre, each parasitic element can behave as a reflector if shortened to the ground plane, that is if the diode from Fig. 4.7 is activated. Thus reflection of the beam towards different directions occurs.

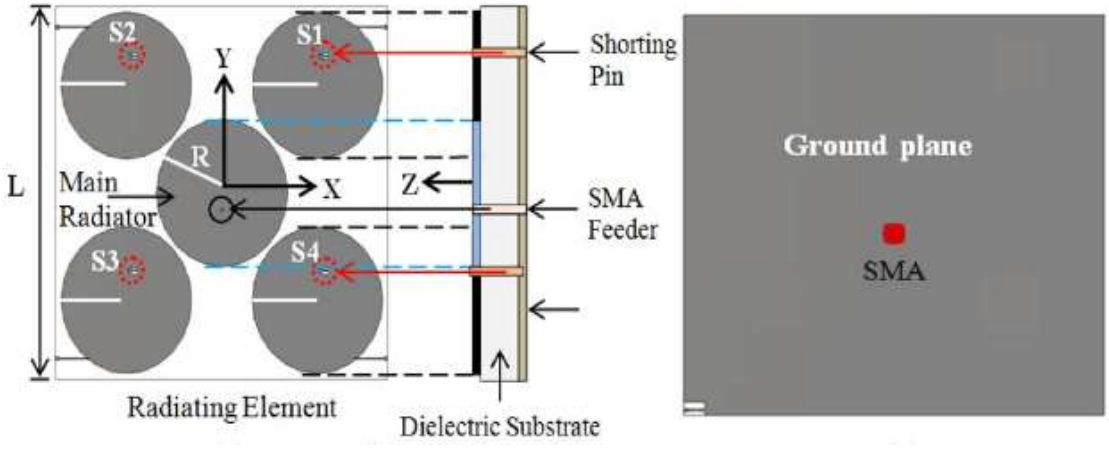

Fig. 4.7 Antenna configuration from Jusoh. M.

However the antenna is bandwidth limited and maximum steering angle limited, making it unfeasible to support high data rates. Note that all the above mentioned RA are single polarized. Dual-polarized antennas have the capability of increasing system capacity and mitigating multipath fading effects, they have been commonly employed as the base station antennas, an example of dual polarized RA can be seen in Fig. 4.8 :

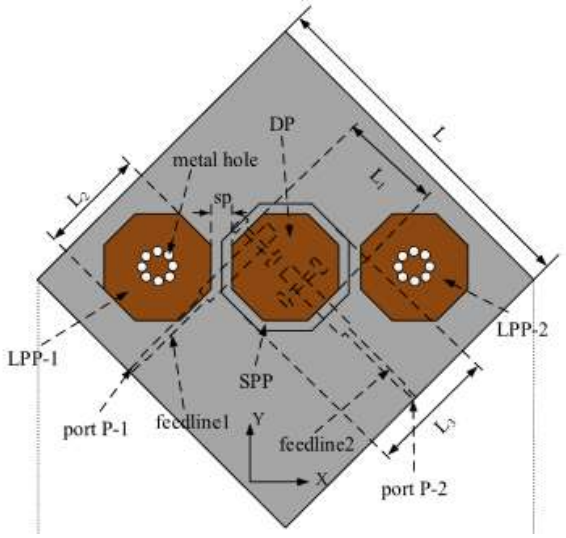

Fig. 4.8 Dual Polarized beam-steering RA for microbase station [30]

By using two orthogonal microstrip lines as the feeding network, and two H slots as aperture coupling, both horizontal and vertical polarization as well as high isolation between ports 1 and 2 is achieved. The steering mechanism is similar to [14], reflective behaviour of both hexagonal parasitic patches can be acquired by shortening them with the ground plane. Although they use 4 switches to achieve only 3 different directions, the novelty of this antenna relies in accomplishing beam-steering for both orthogonal polarizations at the same time.

Table 4.1 summarizes the main features of the exposed antennas. There are three extra rows which corresponds to the different antennas designed during this thesis and can be found in sections 5.1, 5.2 and 5.3.

Works	Nº modes	Nº switches	Pattern reconf.	Pol.	Steering Range	Average Gain(dB)	η(%)	Freq. Range (Ghz)
[12]	12	6	Yes	Sing.	40	8	81	4.9-5.1
[7]	9	12	No	Sing.	30	6.5	N/A	2.4-2.5
[11]	30	12	Yes	Sing.	60	6	N/A	1-6
[14]	9	4	No	Sing.	24	7.5	75	2.36-2.39
[30]	6	4	Yes	Dual	17	6	N/A	3.32-3.51
5.1	**9**	**4**	**No**	**Sing.**	**42**	**9**	**90**	**3.4-3.7**
5.2	**19**	**6**	**Yes**	**Sing.**	**45**	**10**	**95**	**3.3-3.9**
5.3	**18**	**8**	**No**	**Dual**	**20**	**8**	**90**	**3.3-5**

Table 4.1 Comparison of the exposed antennas with the RAs designed during this thesis

As we can see from the above table, we succeed to design three RAs showing wider operation bandwidth, higher efficiency, higher average gain, larger steering angles with a very reduced number of switches.

5. 3D Beam Steering Reconfigurable Antenna

Our initial goal for the thesis was getting the following U-V plane from Figure 5.1, which is simply the projection of the different radiation pattern modes of a RA in the $u = \sin(\theta)\cos(\Phi)$, $v = \sin(\theta)\sin(\Phi)$ axis.

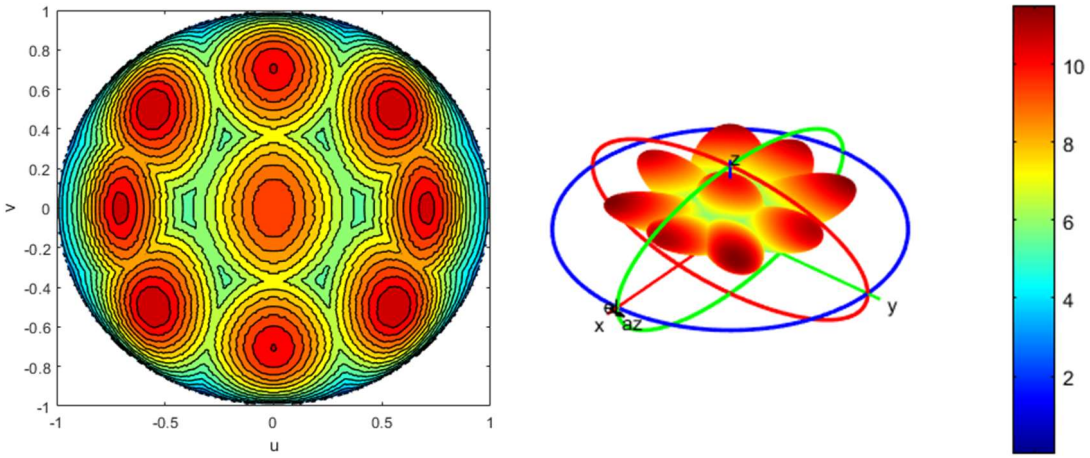

(a) (b)

Fig. 5.1. 3D Radiation pattern (b) goal projected in the UV-plane (a) .

We can appreciate the nine desired modes of operation with maximum beam pointing at:

Mode	θ_{max}	Φ_{max}	Gain(dB)
0	0°	0°	10.25
1-2	$\pm$45°	0°	10.25
3-4	$\pm$45°	90°	10.25
5-8	$\pm$35°	$\pm$35°	10.25

Table 5.1 Beam pattern goal characteristics

In this chapter, the principal design of the antenna for the thesis is presented (section 5.1), followed by a second one (section 5.2) which is an improved version of the previous one and a third design (section 5.3) including beam-steering a double polarized RA. For 5.1, theoretical analysis, simulations and prototyping for the measurements were carried out, showing great accordance between their results. However for 5.2 and 5.3, due to time issues, results were only done at simulation level but showing better results than the initial objective from Fig 5.1.

The first RA consists in exploiting the minimum number of switches possible to achieve maximum spatial diversity. With only four parasitic elements incorporating one switch each one, they are arranged in a new multilevel geometry which allow us to get the nine modes of operation while keeping the antenna simple, compact and elegant. The second one uses the same geometry but aims to improve the radiation patterns of the previous RA by just increasing two switches, totalling six, the number of modes is doubled to eighteen. The last design consists in using the same idea of reconfigurability but by placing crossed parasitic dipoles, with a total number of eight switches we succeed to 3D beam-steering for both orthogonal polarizations. Although the designs may vary among them, the working principle remains the same and can be understood with the theoretical analysis done for the principal RA from 5.1.2.

5.1 Design of the antenna

5.1.1 Geometry of the Antenna.

The RA whose structure is shown in Figure 6.2, 6.3 and 6.4, is mainly composed by a ground plane ($W_g x W_g$) and 3 layers. The substrate used for each layer was the Rogers 3003C ($\varepsilon_r = 3$) of thickness 0.5mm because of its rigidity. Each layer is separated by using nylon screws, leaving an air gap between them. An active dipole with length L_a and width a was placed at the middle layer $(0,0,h_1)$, a coaxial probe was introduced from below the ground plane to feed this dipole, jointly a quarter wavelength Balun [32] was designed in order to symmetrize the currents, providing good impedance matching . This active element is surrounded by four parasitic dipoles with the same width a, two of them (S1 and S2) in the upper layer at $(\pm d_x, 0, h_2)$ with length L_a, and the other ones (S3 and S4) with a shorter length L_d at $(0, \pm d_y, h_0)$, see Fig. 5.2.

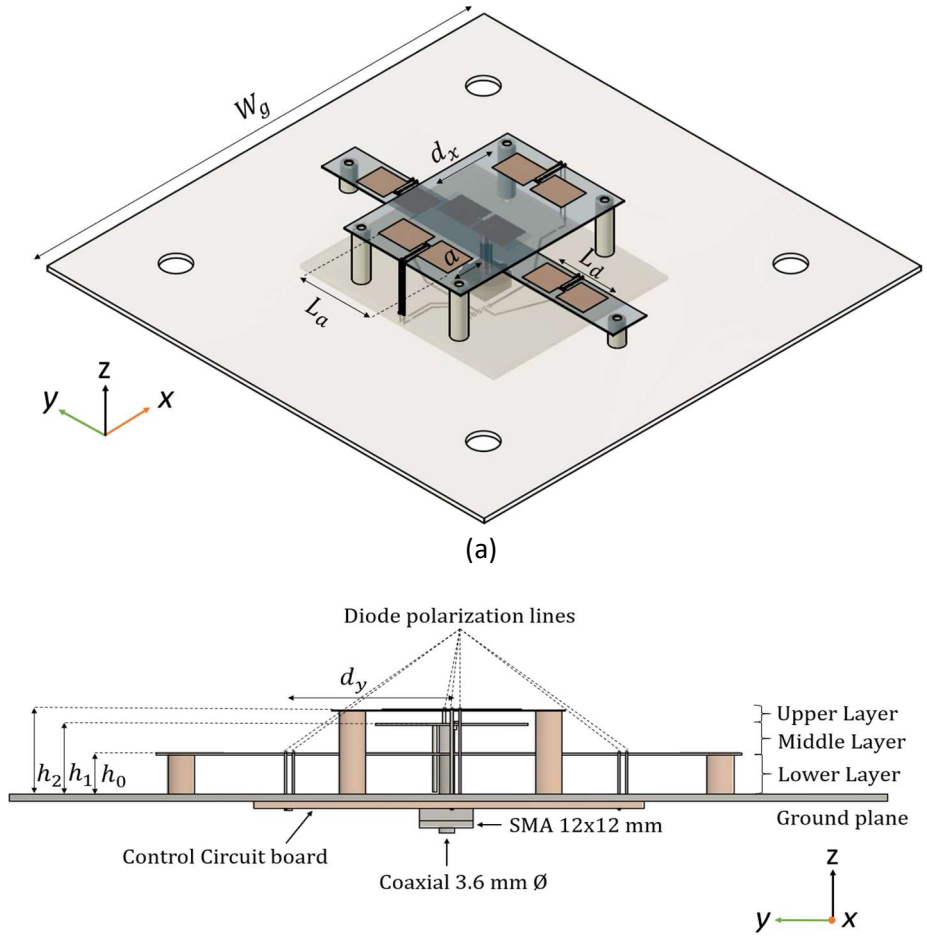

Fig. 5.2. Artist view of the antenna, isometric view (a) and lateral view (b).

By activating a PIN diode-based switch that connects the arms of the parasitic dipoles, a change in their electrical length occurs and a significant current is induced on it, contributing to the total radiation with a relative phase and intensity with respect to the active element. This phase (similarly to the Yagi-Uda concept) and the multilevel geometry are responsible for directionally orienting (steering) the beam in a certain direction. When the switch is on its OFF state, the current induced on each parasitic is negligible at the frequency of interest.

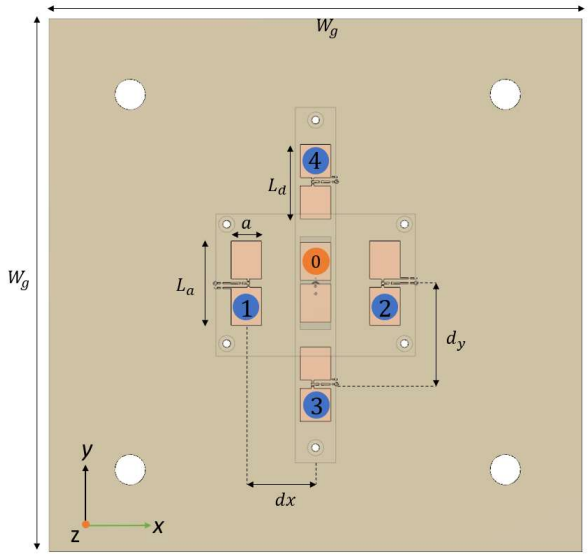

Fig. 5.3. Top View

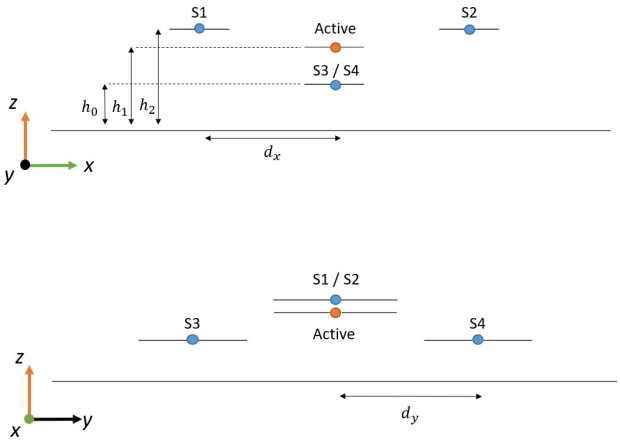

Fig. 5.4. Front View and Side View

The dimensions of the different antenna parameters are listed in the table below :

L_a	0.39 λ	W_g	2.4 λ
L_d	0.342 λ	h_0	0.123 λ
a	0.14 λ	h_1	0.21 λ
d_x	0.32 λ	h_2	0.25 λ
d_y	0.455 λ	*Coaxial*	3.6 mm Ø

Table 5.2. Dimensions of the antenna parameters.

Each parasitic dipole has a switching mechanism, which is composed by two main elements, an inductor and a diode :

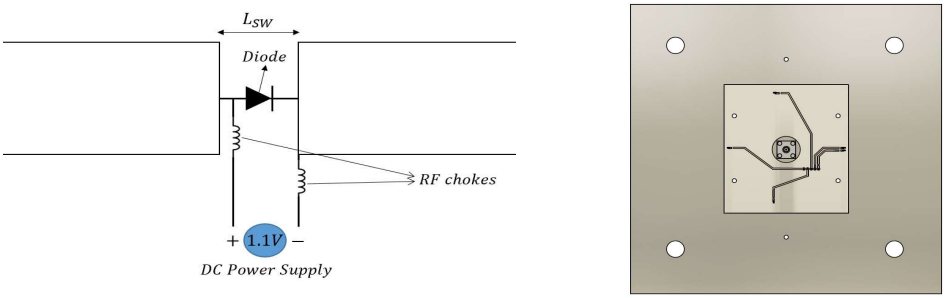

Fig. 5.5. In the left hand side, the switching mechanism for each parasitic element and in the right hand side the control circuit of the polarization of each diode.

The polarization lines of the diodes are connected to each reconfigurable dipole by means of Ø 0.5 mm metallic wires from below the ground plane, where a low frequency circuit printed on a FR4 substrate was designed for controlling each diode state. A total amount of 19 Murata 10 nH inductors (LQG18HN10NJ00D) with minimum resonant frequency of 3.5 GHz were located at strategic positions in order to decouple as much as possible the RF signal from the DC signal. Also, 4 Infineon BAR64 Series diodes (BAR6402VH6327XTSA1) are used as switches providing an

isolation of 15 dB and less than 0.3 dB insertion losses at the resonant frequency. An Arduino micro-controller is placed in the back to control the different modes of operation of the RA.

A prototype of the antenna, illustrated in Figure 5.6 was manufactured using standard PCB technology, and measured at the UPC facilities .

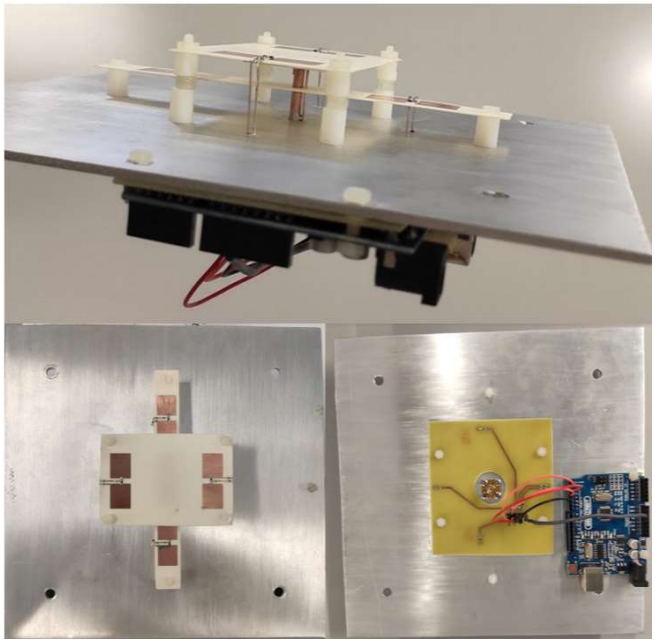

Fig. 5.6 Manufactured antenna

5.1.2 Working Principle

The directional capability of the multilevel phasing concept, stated in the previous section, when combined with a ground plane produces additional upwards reflected beam increasing up to 9 the directional modes of operation, summarized in Table 5.4. In this section an intuitive mathematical formulation combining the use of mutual impedances, array factor and image theory is presented and validated for all the modes of operation.

Mode	S1	S2	S3	S4
0	Off	Off	Off	Off
1	Off	On	Off	Off
2	On	Off	Off	Off
3	Off	Off	Off	On
4	Off	Off	On	Off
5	Off	On	Off	On
6	On	Off	On	Off
7	On	Off	Off	On
8	Off	On	On	Off

Table 5.4. Configuration of the different 9 modes.

Starting for the mode 0 (broadside radiation) where no switches are activated, the radiated field is just given by the array factor composed by the driven dipole element with its image:

$$\overrightarrow{E_0}(\theta,\Phi) = \overrightarrow{E_{dip}}(\theta,\Phi)\, I_0\left(e^{j\,k_z h_1} - e^{-j\,k_z h_1}\right) \qquad (5.1)$$

Where I_0 and $\overrightarrow{E_{dip}}(\theta, \Phi)$ are the current and the electric field in free space of the driven element.

Regarding the case of having only one parasitic element activated, which corresponds to the modes 1,2,3,4, the voltages and currents in the driven dipole and parasitic ones are related by the impedance matrix Z as done in [13], [33] and [34] :

$$\begin{pmatrix} V_0 \\ I_m X \end{pmatrix} = \begin{pmatrix} Z_{00} & Z_{0m} \\ Z_{m0} & Z_{mm} \end{pmatrix} \begin{pmatrix} I_0 \\ I_m \end{pmatrix} \tag{5.2}$$

Regarding the second row :

$$I_m X = Z_{m0} I_0 + Z_{mm} I_m \tag{5.3}$$

The relative phase between the active element and the parasitic one is α:

$$\frac{I_m}{I_0} = \frac{Z_{m0}}{X - Z_{mm}} = A_{m0} e^{j\alpha_{m0}} \tag{5.4}$$

Where X is the impedance of the diode at the frequency of operation. 0 and m subscripts corresponds to the driven and parasitic elements respectively. The mutual impedances Z_{m0} and self-impedance Z_{mm} must be computed numerically. Depending on whether the relative phase α_{m0} is positive or negative, the parasitic elements will act as either reflector or director. The position of the two parasitic dipoles at the upper layer were optimized numerically in order to act as reflectors and the ones at the lower layer as directors by shortening the length. As the intrinsic directive behaviour of a shorter dipole element in the axis of the driven element $\hat{y}$ was not enough to steer the beam towards $\Phi = \pm 90°$, which corresponds to a null radiation direction from a dipole element in free space located parallel to $\hat{y}$ axis, we needed a higher capacitive effect in order to make it more directive. That was achieved by approximating them towards the ground plane at h_0. Once we know the relative phase α_{m0}, by applying image theory again the radiated fields are then:

$$\overrightarrow{E_m}(\theta, \Phi) = \overrightarrow{E_0}(\theta, \Phi) + \overrightarrow{E_{dip}}(\theta, \Phi) \frac{I_m}{I_0} \left(e^{j(\vec{k}\overrightarrow{d_m} + k_z h_2)} - e^{j(\vec{k}\overrightarrow{d_m} - k_z h_2)} \right) \tag{5.5}$$

Note that $\overrightarrow{d_m}$ are the position of the parasitic elements at z=0, and subscript m denotes the mode of operation corresponding to 1,2,3,4 in this case.

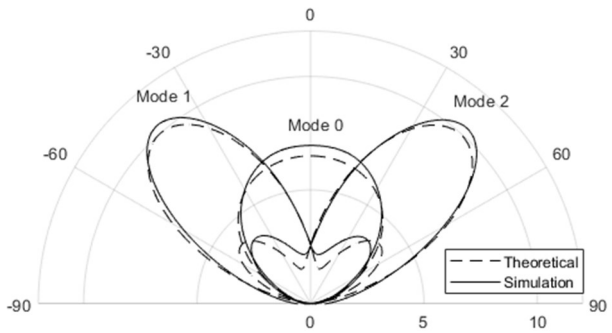

X	0Ω
Z_{21}	$27.15 - j21.7\ \Omega$
Z_{22}	$62.8 - j14.15\ \Omega$
α	$62.8°$

Fig. 5.6. Polar plot of the radiation pattern in linear at $\Phi = 0°$ for modes 0,1 and 2.

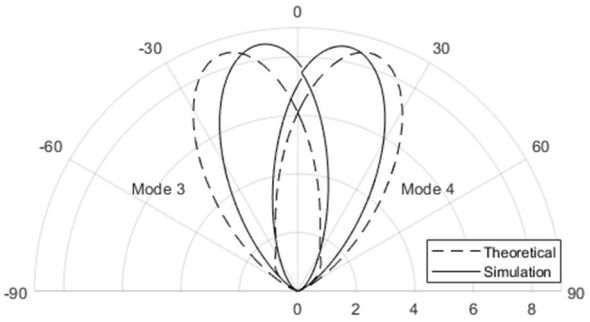

X	0Ω
Z_{21}	$17\ + j7.5\ \Omega$
Z_{22}	$18\ - j28.7\ \Omega$
α	$-98.23°$

Fig. 5.7. Polar plot of the radiation pattern in linear at $\Phi = 90°$ for modes 3 and 4.

We can clearly see the Yagi-Uda antenna concept, the parasitic element acts as reflector whenever α is positive, and reflector when it is negative. Regarding the modes n = 5,6,7 and 8 where two parasitic elements are activated at the same time, their interaction can be calculated in the same way as follows :

$$\begin{pmatrix} V_0 \\ I_m X \\ I_n X \end{pmatrix} = \begin{pmatrix} Z_{00} & Z_{0m} & Z_{0n} \\ Z_{m0} & Z_{mm} & Z_{mn} \\ Z_{n0} & Z_{nm} & Z_{nn} \end{pmatrix} \begin{pmatrix} I_0 \\ I_m \\ I_n \end{pmatrix} \tag{5.6}$$

Solving the linear system of equations given by second and third row we arrive to the following expressions :

$$\frac{I_n}{I_0} = \frac{Z_{m0}Z_{nm} + Z_{n0}(X - Z_{mm})}{(X - Z_{mm})(X - Z_{nn}) - Z_{mn}Z_{nm}} \tag{5.7}$$

$$\frac{I_m}{I_n} = \frac{\frac{I_n}{I_0}(X - Z_{nn}) - Z_{n0}}{Z_{nm}} \tag{5.8}$$

and its corresponding radiated fields are :

$$\overrightarrow{E_{m,n}}(\theta, \Phi) = \overrightarrow{E_m}(\theta, \Phi) + \overrightarrow{E_{dip}}(\theta, \Phi) e^{j\vec{k}\vec{d_n}} \left(e^{jk_z h_1} - e^{-jk_z h_1} \right) \tag{5.9}$$

Where now, m can only correspond to the parasitic from mode 1,2 and n to the ones from mode 3,4. The combination of two nearest m and n parasitic elements yields the 5,6,7,8 modes.

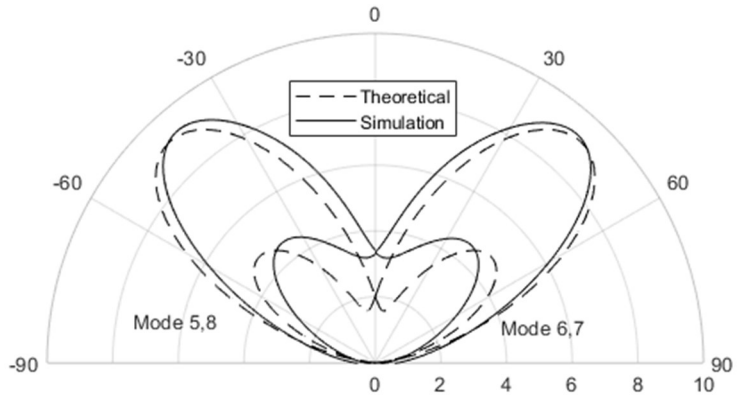

Fig. 5.8. Polar plot of the radiation pattern in linear at $\Phi = 0°$ for modes 5,6,7 and 8.

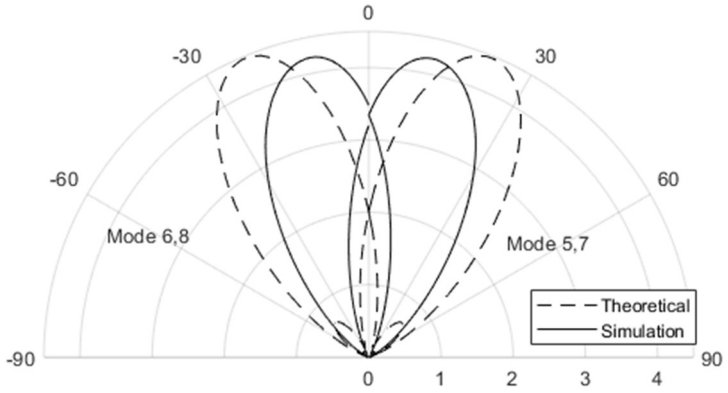

X	0Ω
Z_{m0}	$27.33 - j22.9\ \Omega$
Z_{nm}	$7.58 - j7.79\ \Omega$
Z_{mm}	$57 - j11.8\ \Omega$
Z_{n0}	$17 - j7.5\ \Omega$
Z_{nn}	$18 - j28.7\ \Omega$
Z_{mn}	Z_{32}
$\alpha_{0,n}$	$140.8°$
$\alpha_{n,m}$	$-81°$

Fig. 5.9. Polar plot of the radiation pattern in linear at $\Phi = 90°$ for modes 5,6,7 and 8.

A good agreement between the computed analytical solution with respect to the simulated one is obtained. This theoretical approach is more accurate the bigger the ground plane is as image theory assumes an infinite ground plane.

5.1.3 Experimental Results

A comparison between the results from a full electromagnetic simulation tool (CST) and the measurements in the anechoic chamber at the UPC facilities for the different modes is shown in this section. Simulation and measurements included the input reflection coefficient and the far field radiation patterns.

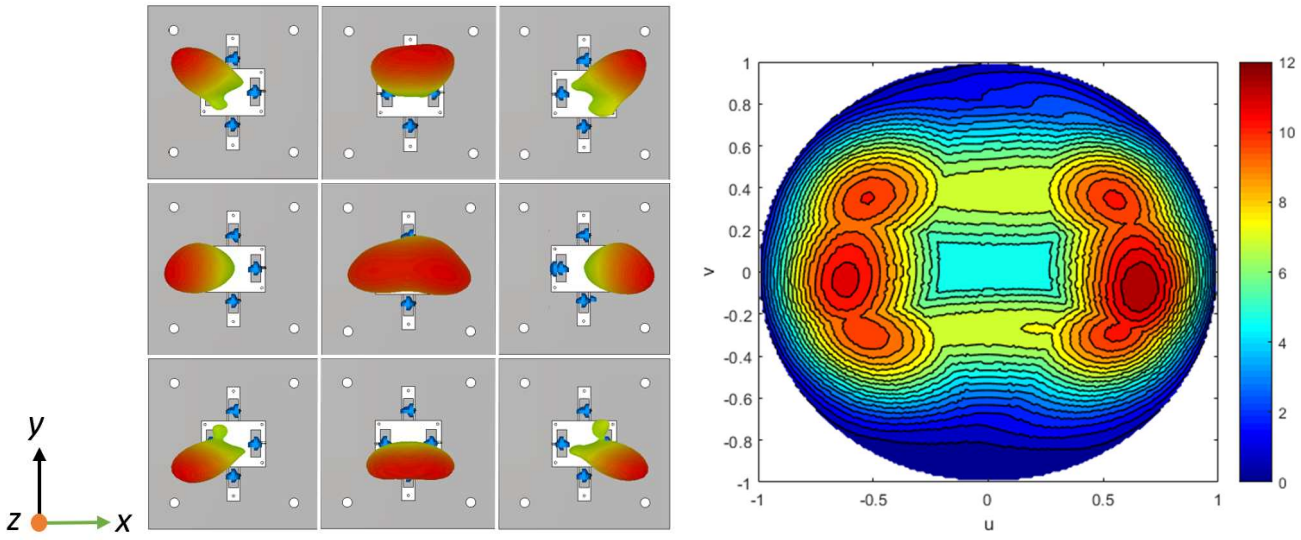

(a) (b)

Fig. 5.10. (a) Simulated radiation pattern in linear and (b) projected in u-v plane for all the 9 modes of operation.

Measurements were carried out for only 4 modes, corresponding to 0, 1, 3 and 5, the rest ones are symmetric, showing a good agreement with the simulated results in Fig. 5.12 and 5.13.

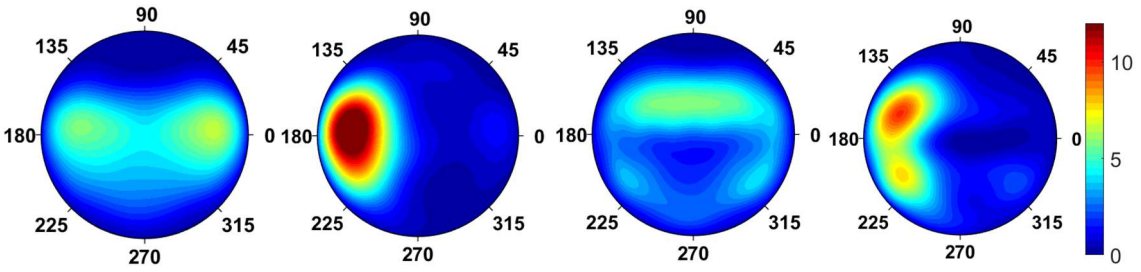

Fig. 5.11. UV plane projection of the measured 3D radiation patterns in the anechoic chamber. (a) mode 0, (b) mode 1 , (c) mode 3 , (d) mode 5

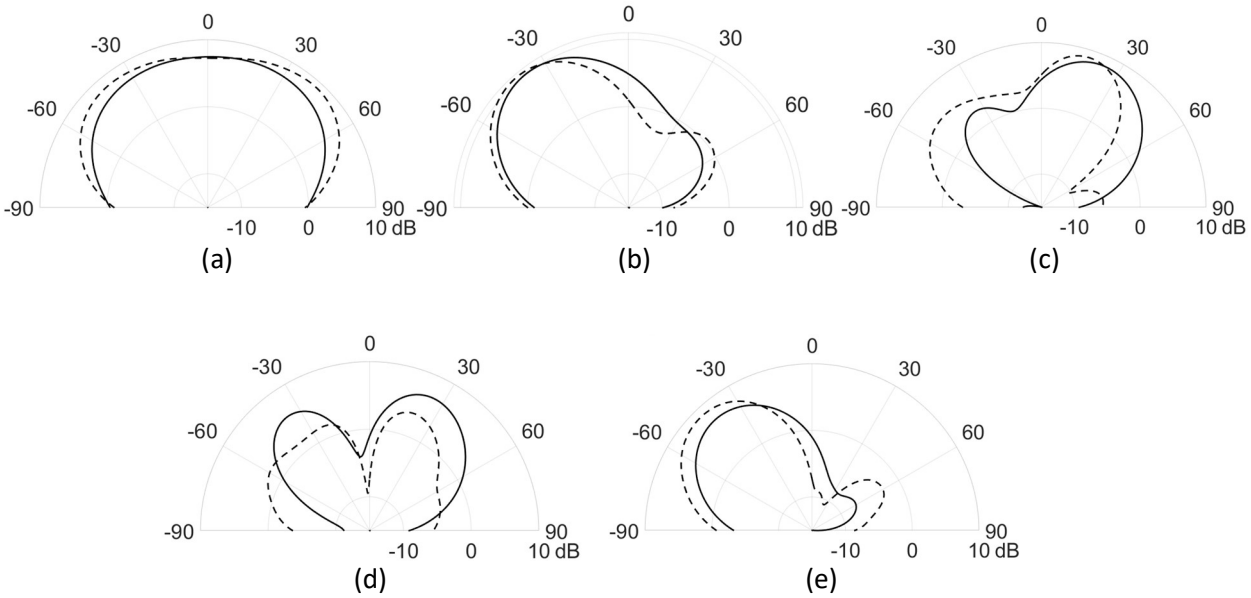

Fig. 5.12 Polar plot in dB of the simulated – and measured - - radiation pattern. ZY plane cut for (a) Mode 0, (b) Mode 1, (c) Mode 3, (d) Mode 5 and ZX plane cut for (e) Mode 5.

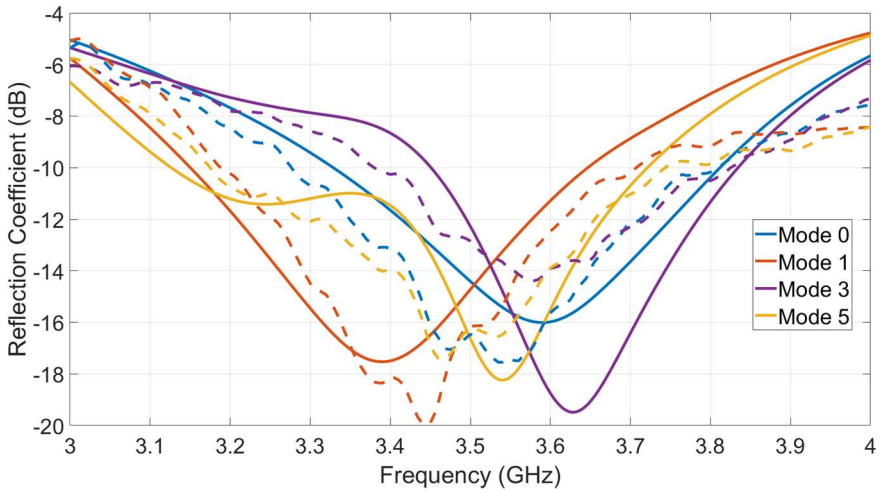

Fig. 5.13. Simulated and measured results for modes 0,1,3 and 5.

The different modes cover the bandwidth 3.4-3.8 GHz (just mode 1 is 1dB above -10 dB from 3.7 to 3.8 GHz), and the maximum realized gain of 10.6 dB is achieved. We can see from the S_{11}

parameters of Fig. 5.13 that the switches from the upper layer reduces the resonant frequency while the switches from the lower layer shifts up the resonant frequency, and if we activate both of them we have an ultrawideband mode. The more capacitive is the parasitic element the higher shift of this resonant frequency and it is more inductive for the other way.

In general there is a trade off between the length of the parasitic dipoles, the height, steering angle, secondary lobes (for example Mode 1 and 5) and bandwidth. An important issue is the study of the gain stability as reported in [7] and [14]. In this RA, again a trade off between gain and steering angle must be faced. A simple solution to achieve both would be reactively loading the switches with capacitors/inductors as first mentoned by R. Harrington [2], so we can keep all the parasitic elements reflective/directive in a higher layer with more stable gain.

$Mode$	$Gain(dB)$	θ_{max}	Φ_{max}	$BW(GHz)$	η (%)
0	7.2	$0°$	$0°$	3.28-3.8	92.45
1	10.6	$-42°$	$0°$	3.2-3.7	93.11
3	8.57	$25°$	$90°$	3.4-3.82	87.31
5	9.8	$42°$	$155°$	3.12-3.72	91.1

Table 5.5. Results of the measured farfield pattern.

The above table shows a summary about the main features of the RA for the different measured modes of operation. Efficiency was taken from the simulations.

The antenna is suitable for 5G New Radio (NR) Frequency Range (FR) 1 applications where broadband, high directivity, high efficiency and beamforming can be translated into higher capacity.

5.2 Radiation Pattern improvement

As seen in the previous chapter, the results of the beam pattern for the broadside direction and $\pm\, y\ axis$ was not that directive. In this section we will show the simulation results of an antenna with improved steering capabilities by adding only two more parasitic dipoles in the first layer at $(\pm\, 2d_x\ , 0, h_0)$ acting as reflectors, see Figure 5.14 (a). With this simple addition we achieved 19 different modes of operation see Figure 5.15, more steering resolution and pattern reconfigurability at $\pm\, y$.

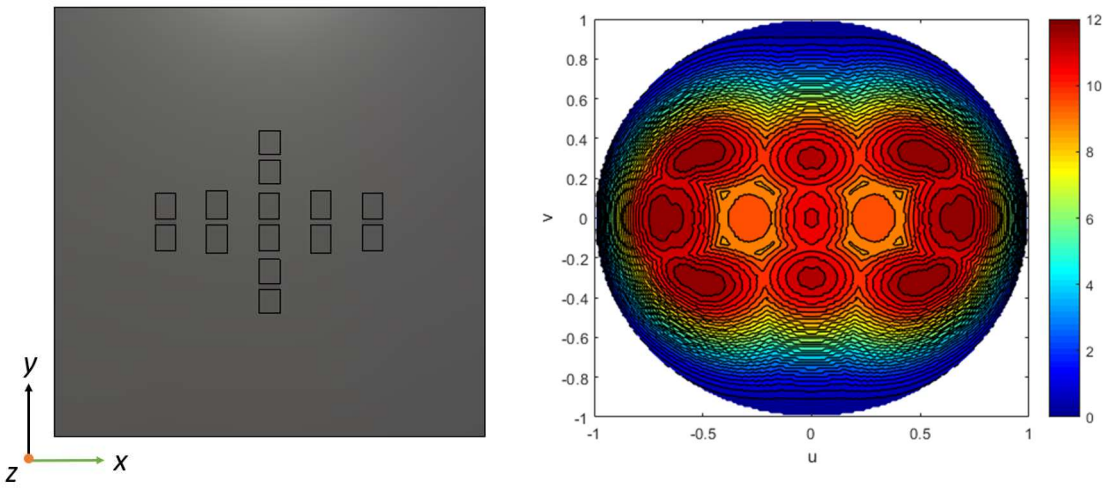

(a) (b)

Fig. 5.14. (a) Top View of the improved antenna and (b) far field radiation pattern for the 19 modes of operation projected in the U-V plane.

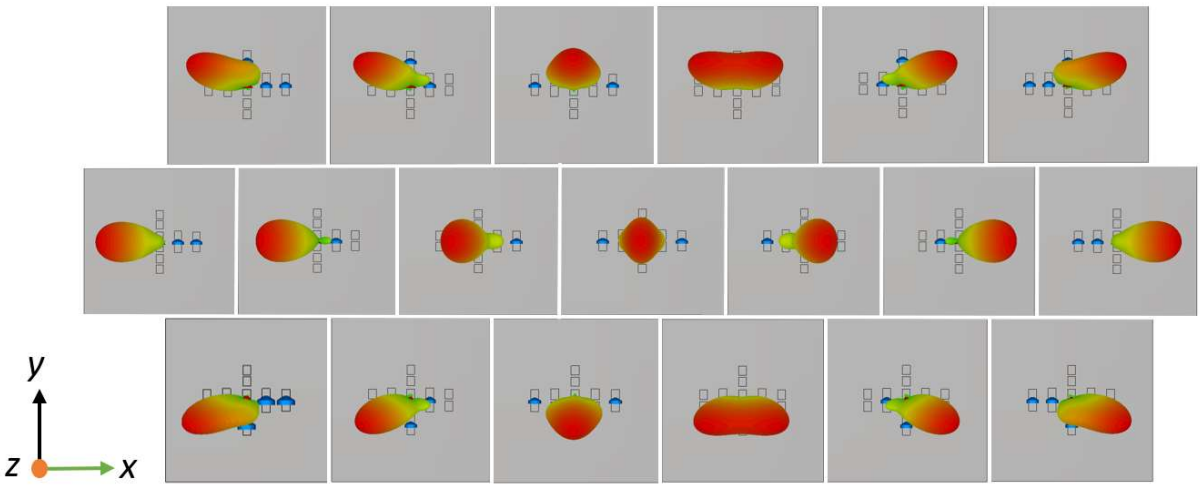

Fig. 5.15. Far field radiation pattern for each mode of operation.

We can appreciate from the previous figure that the steering angle and directivity in $\hat{y}$ direction is improved because a higher number of parasitic elements are activated, composing an array of more elements. It also has the capability to provide a wider beam which can be very useful to

increase coverage in that direction. Furthermore, broadside's directivity is highly increased from 7.2 dB to 11dB.

For the $\hat{x}$ directions, we succeed to get more steering angles corresponding to $17°$, $39°$ and $44°$ with high directivity, 9.73-12.1 dB depending on the mode of operation, see Table 5.6. The same as for diagonal directions, totalling 8 modes for these directions with an average directivity of 10.8 dB, see Table 5.8.

$Mode$	$Gain(dB)$	θ_{max}	Φ_{max}	η (%)
0	11	$0°$	$0°$	98
1	9.73	$17°$	$0°$	99.2
2	9.73	$-17°$	$0°$	99.2
3	11.5	$39°$	$0°$	97.7
4	11.5	$-39°$	$0°$	97.7
5	12.1	$44°$	$0°$	97
6	12.1	$-44°$	$0°$	97

Table 5.6. Results for the $\pm\, x$ steering modes.

$Mode$	$Gain(dB)$	θ_{max}	Φ_{max}	η (%)
7	10.6	$20°$	$90°$	90
8	10.6	$-20°$	$90°$	90
9	8.63	$20°$	$90°$	92
10	8.63	$-20°$	$90°$	92

Table 5.7. Results for the $\pm\, y$ steering modes.

$Mode$	$Gain(dB)$	θ_{max}	Φ_{max}	η (%)
11	10.8	$39°$	$20°$	94
12	10.7	$45°$	$20°$	94
13	10.8	$39°$	$160°$	94
14	10.7	$45°$	$160°$	94
15	10.8	$39°$	$-20°$	94
16	10.7	$45°$	$-20°$	94
17	10.8	$39°$	$-160°$	94
18	10.7	$45°$	$-160°$	94

Table 5.8. Results for the diagonal steering modes.

The efficiencies are very high because we didn't simulate the antenna with the inductors for DC isolation, neither with the model of the PIN diode which introduces some losses (around 0.2dB per diode). The polarization lines of the PIN diodes was not incorporated in the simulations as they don't really affect the radiated patterns neither the S_{11} parameters, this is already proved with simulations and real measurements in the anechoic chamber for the previous design. For that reason, if manufacturing properly, all the measured results should be in accordance with the simulated results.

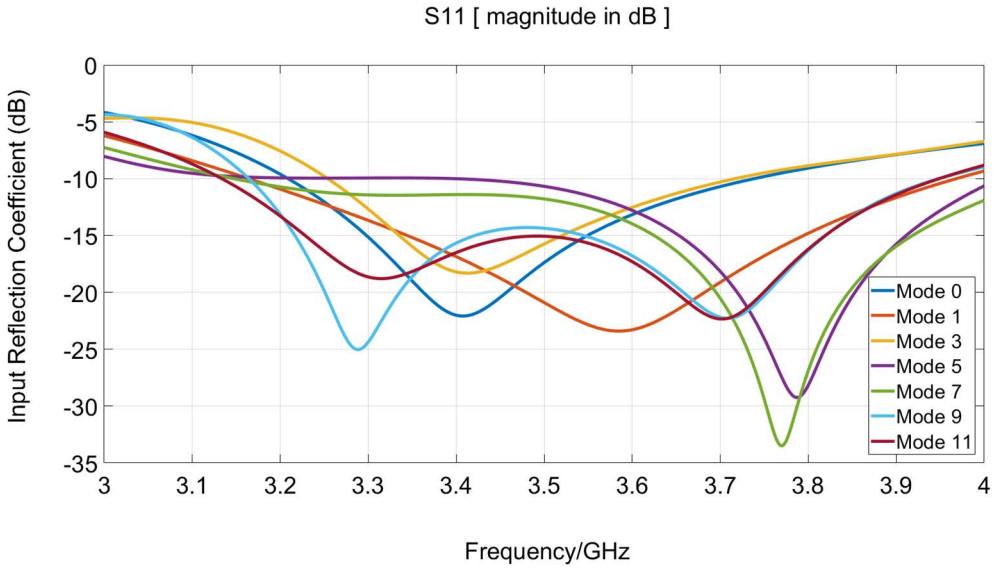

Fig. 5.16 Simulated input reflection coefficient for the principal modes of operation. The rest ones are symmetric.

The antenna works in the whole 3.3-3.7 GHz band which makes it suitable for 5G-New Radio applications. In order to increase the bandwidth of the system, a simple way would be replacing the dipoles by bow-ties [35].

The figure from below shows a comparison of the steering characteristics for the initial antenna from previous section, the improved one from this section with the initial objective.

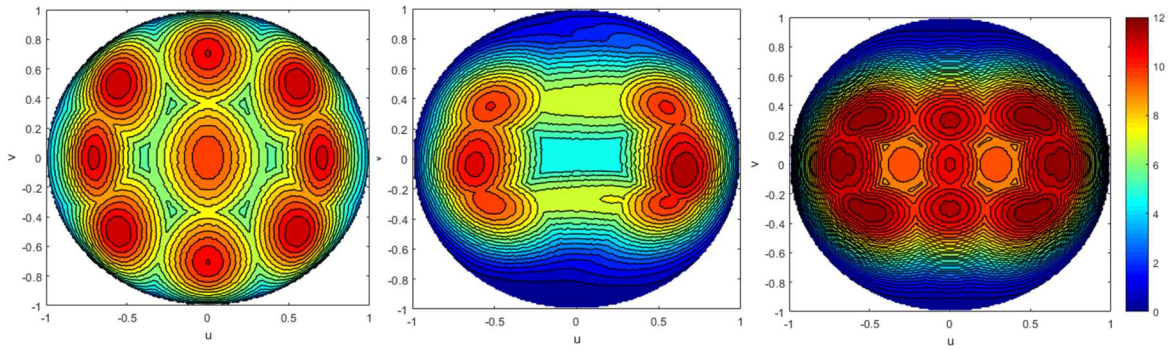

Fig. 5.17 Far field projection in the U-V plane for all the modes of operation. (a) For initial objective result, (b) section 5.1 antenna using 4 switches and (c) improved antenna using 6 switches.

In conclusion, overall steering capability is highly improved, as well as gain and coverage by just adding two switches which is simply translated into an antenna with higher reliability able to support huge amount of data rates.

5.3 Dual Polarized 3D Beam-Steering antenna

In this last section, we present a dual polarized (DP) RA, providing 3D beam steering in 9 different directions for each vertical and horizontal polarization. As they usually need double number of components for achieving polarization diversity, mobile phones normally incorporate single polarized antennas for compactness issues. That's why dual-polarized antennas are widely used in base stations to guarantee reliable mobile communication, specially for LOS cases where communication between two single polarized devices may drop completely because of their misalignment.

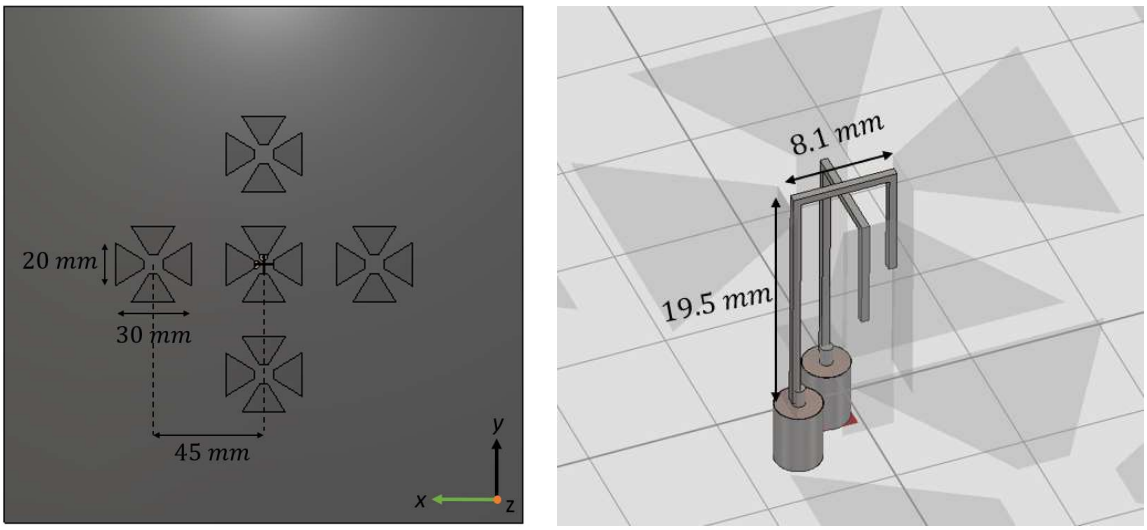

(a) (b)

Fig 5.18 (a) Top view of the DP antenna (b) DP Gamma feeding.

The active crossed dipole elements at (0, 0, 19.5) mm, are fed by implementing a gamma like metallic structure [36] which provides a compact way for feeding two crossed geometries. Low mutual coupling between the two ports and a high fractional bandwidth (FBW) (50 %) can be achieved, see Figure 5.18.

There are eight crossed parasitic Bow-tie antennas at an upper layer that acts as reflectors, half of them that are oriented to $\hat{x}$ for steering horizontal polarization are at 24 mm, which will be printed below a RO4003 substrate. The other four parasitic elements are oriented to $\hat{y}$ for steering vertical polarization and are located at a higher level above the substrate at 24.5 mm, in this manner the diodes for both polarizations that interconnects each Bow-tie's arm are separated. A total amount of 8 PIN diodes is required.

$Mode$	θ_{max}	Φ_{max}	$Gain\ (dB)$
0	0	0	7.8
1	30	0	9
2	45	45	9.35
3	30	90	8.45

Table 5.9 Features for Vertical polarization

$Mode$	θ_{max}	Φ_{max}	$Gain\ (dB)$
0	0	0	7.8
1	30	0	9.30
2	45	45	8.55
3	30	90	8.52

Table 5.9 Features for Horizontal polarization

The simulated S11, S22 and S12 parameters for the different Modes of operation are :

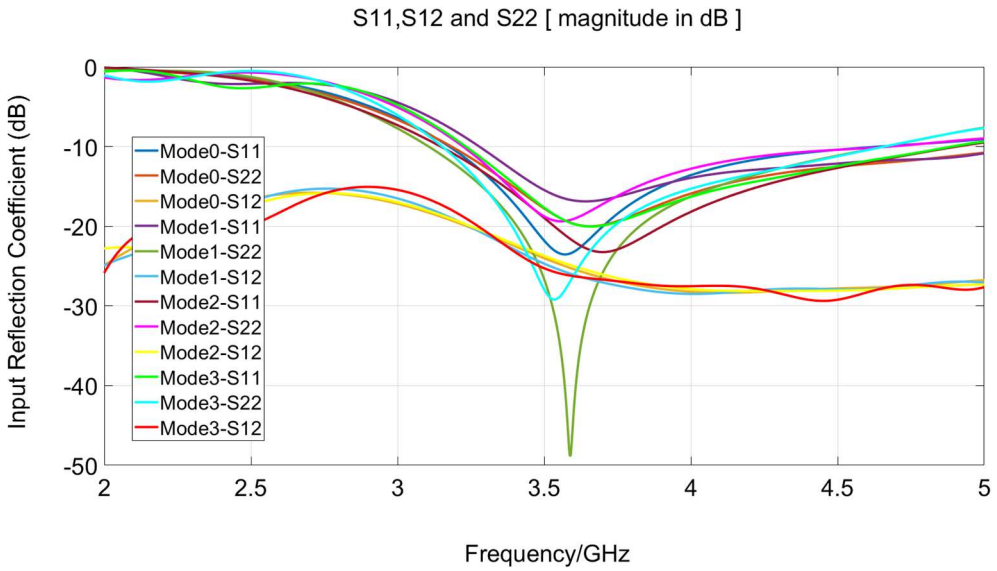

Fig. 5.19 Reflection coefficient with the 4 nonredundant modes of operation.

The rest of the modes 4-8 are not symmetric due to the asymmetry of the gamma feeding structure. Although the steered angles are symmetric the gains towards $+\hat{x}$ is decreased approximately 0.5 dB with respect to the ones to $-\hat{x}$.

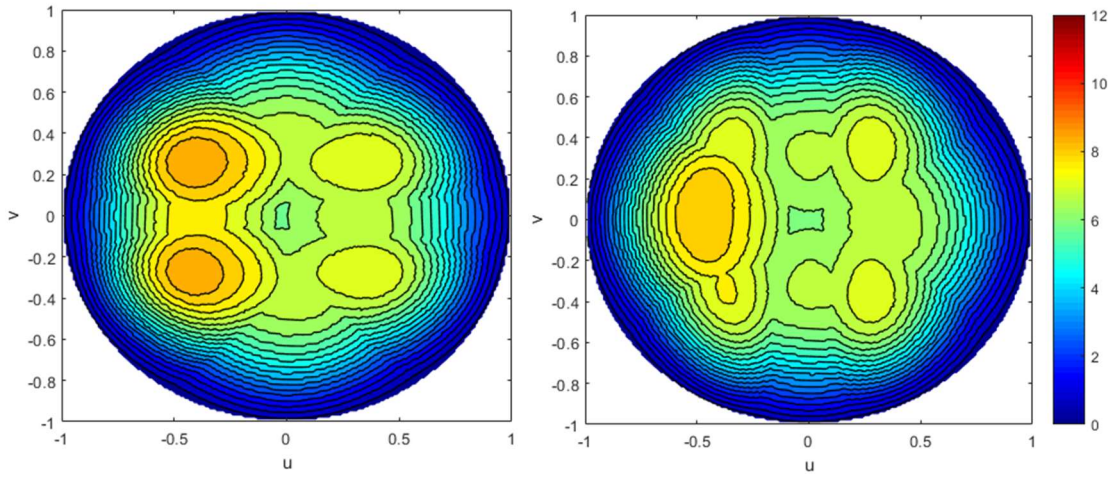

(a) (b)

Fig. 5.20 Far field showing the 9 different modes of operation for both (a) horizontal polarization and (b) vertical polarization.

The antenna is suitable for 5G NR FR1 applications, concretely for base stations where polarization diversity is very important for a robust communication. A complete design of the antenna for fabrication should be considered to fully validate the simulated concept.

6.Conclusions

A novel low complexity multilevel reconfigurable antenna was designed and proved with a rigorous theoretical analysis, simulations and measurements. The antenna uses the lowest number of PIN diodes as switches possible while keeping a large amount of coverage, that is achieving nine different directions. It is possible to reduce this number of switches by using 2 varactors as switches instead of diodes, composing a canonical base for steering into any directions changing the capacitance of the varactor diode.

Improvements of the antenna was performed at simulation level, by just adding two more switches the antenna's modes was doubled up to 18 instead of 9. This new configuration highly enhanced the steering characteristics of the primitive antenna, offering beam width variability, high directivity and more steering steps.

At the end of this thesis, a double polarization reconfigurable antenna for beam steering was designed and proved with the simulations. Offering excellent isolation for both ports, and nine different directions for both polarizations.

Future works may consist in optimizing the antenna's steering performance for a smaller ground plane and improve the steering stability in the band of operation, that could be done by reactively loading the switches, so we can keep all the parasitic elements at an upper layer, while being able to steer the beam with decent stability into the corresponding nine different directions.

7. REFERENCES

[1] Uchendu, I., & Kelly, J. (2016). Survey of beam steering techniques available for millimeter wave applications. Progress In Electromagnetics Research B, 68(1), 35–54.

[2] Harrington, R. (2005). Reactively controlled antenna arrays. 3, 62–65.

[3] Gyoda, K., & Ohira, T. (2000). Design of Electronically Steerable Passive Array Radiator (ESPAR) antennas. IEEE Antennas and Propagation Society, AP-S International Symposium (Digest), 2, 922–925.

[4] Gu, C., Gao, S., Zhang, M., Xu, L., Sanz-Izquierdo, B., & Sobhy, M. (2014). Design of broadband ESPAR antenna using inverted F monopoles. 8th European Conference on Antennas and Propagation, EuCAP 2014, EuCAP, 1814–1817.

[5] Rodrigo, D., Cetiner, B. A., & Jofre, L. (2014). Frequency, radiation pattern and polarization reconfigurable antenna using a parasitic pixel layer. IEEE Transactions on Antennas and Propagation, 62(6), 3422–3427.

[6] Towfiq, M. A., Khalat, A., Blanch, S., Romeu, J., Jofre, L., & Cetiner, B. A. (2019). Error Vector Magnitude, Intermodulation, and Radiation Characteristics of a Bandwidth- and Pattern-Reconfigurable Antenna. IEEE Antennas and Wireless Propagation Letters, 18(10), 1956–1960.

[7] Li, Z., Ahmed, E., Eltawil, A. M., & Cetiner, B. A. (2015). A beam-steering reconfigurable antenna for WLAN applications. IEEE Transactions on Antennas and Propagation, 63(1), 24–32.

[8] Jung, T. J., Hyeon, I. J., Baek, C. W., & Lim, S. (2012). Circular/linear polarization reconfigurable antenna on simplified RF-MEMS packaging platform in K-band. IEEE Transactions on Antennas and Propagation, 60(11), 5039–5045.

[9] Venneri, F., Costanzo, S., & Di Massa, G. (2013). Design and validation of a reconfigurable single varactor-tuned reflectarray. IEEE Transactions on Antennas and Propagation, 61(2), 635–645.

[10] Yuan, X., Li, Z., Rodrigo, D., Mopidevi, H. S., Kaynar, O., Jofre, L., & Cetiner, B. A. (2012). A parasitic layer-based reconfigurable antenna design by multi-objective optimization. IEEE Transactions on Antennas and Propagation, 60(6), 2690–2701.

[11] Rodrigo, D., Romeu, J., Cetiner, B. A., & Jofre, L. (2016). Pixel reconfigurable antennas: Towards low-complexity full reconfiguration. 2016 10th European Conference on Antennas and Propagation, EuCAP 2016, 1–5.

[12] Towfiq, M. A., Bahceci, I., Blanch, S., Romeu, J., Jofre, L., & Cetiner, B. A. (2018). A reconfigurable antenna with beam steering and beamwidth variability for wireless communications. IEEE Transactions on Antennas and Propagation, 66(10), 5052–5063.

[13] Chamok, N. H., Yilmaz, M. H., Arslan, H., & Ali, M. (2016). High-Gain Pattern Reconfigurable MIMO Antenna Array for Wireless Handheld Terminals. IEEE Transactions on Antennas and Propagation, 64(10), 4306–4315.

[14] Jusoh, M., Aboufoul, T., Sabapathy, T., Alomainy, A., & Kamarudin, M. R. (2014). Pattern-reconfigurable microstrip patch antenna with multidirectional beam for WiMAX application. IEEE Antennas and Wireless Propagation Letters, 13(Mcmc), 860–863.

[15] Technology, U. M. (2001). 2-d mechanical beam steering antenna fabricated using mems technology.

[16] Veen, B. D. Van, & Buckley, K. M. (1988). Beamforming : A Versatile Approach to Spatial Filtering. April.

[17] Gharbi, I., Barrak, R., Latrach, M., Ragad, H., & Menif, M. (2019). Design of a switched line phase shifter for reconfigurable mm-wave Antennas. 2019 15th International Wireless Communications & Mobile Computing Conference (IWCMC), 1440–1444.

[18] Atwater, A. Circuit Design of the Loaded-Line Shifter. IEEE Transactions on Microwave Theory and Techniques 626–634.

[19] Singh, A., Member, S., Mandal, M. K., & Member, S. (2019). Electronically Tunable Reflection Type Phase. IEEE Transactions on Circuits and Systems II: Express Briefs, PP(c), 1.

[20] Castafieda, L. G., Ustairiz, J. C., & Knapp, E. (2006). Phase Shifter System Using Vector Modulation For Phased Array Radar Applications. 0313747, 688–692.

[21] H. Steyskal, "Digital Beamforming," *1988 18th European Microwave Conference*, Stockholm, Sweden, 1988, pp. 49-57.

[22] Godara, L. C., "Application of the fast fourier transform to broadband beamforming," J. Acoust. Soc. Amer., Vol. 98, No. 1, 230–240, Jul. 1995.

[23] Forbes, R., Forbes, R., Forbes, G. R., Shodin, L. F., King, P., Jordan, C., Company, P. B., & York, K. (1963). The Reflectarray Antenna".

[24] Buttgenbach, T. H., & Member, S. (1993). An Improved Solution for Integrated Array Optics in Quasi-Optical mm and Submm Receivers : the Hybrid Antenna. 41(10), 1750–1761.

[25] V.G Veselago (1964). The electrodynamics of substances of simultaneously negative values of ε and μ

[26] Mingle, S., Hassoun, I., & Kamali, W. (2019). Beam-Steering in Metamaterials Enhancing Gain of Patch Array Antenna Using Phase Shifters for 5G Application. IEEE EUROCON 2019 -18th International Conference on Smart Technologies, 1–4.

[27] Abbas, S. M., Esselle, K. P., Matekovits, L., Rizwan, M., & Ukkonen, L. (2016). On-body Antennas : Design Considerations and Challenges (Invited Paper). 2016 URSI International Symposium on Electromagnetic Theory (EMTS), 109–110.

[28] Sharma, M., Parini, C. G., & Alomainy, A. (n.d.). Influence of Antenna Alignment and Line-of-sight Obstruction on the Accuracy of Range Estimates between a Pair of Miniature UWB Antennas. 2015 9th European Conference on Antennas and Propagation (EuCAP), 1–5.

[29] Rodrigo, D., Jofre, L., Unlu, M., Damgaci, Y., Cetiner, B. A., & Romeu, J. (n.d.). Genetic reconfigurability of a multi-size pixelled antenna. 2010 IEEE International Conference on Wireless Information Technology and Systems, 1, 1–4.

[30] Dual-Polarized Pattern Reconfigurable YagiPatch Antenna for Microbase StationsWan-Qiang Deng, Xue-Song Yang,Member, IEEE, Cong-Song Shen, Jianping Zhao,and Bing-Zhong Wang,Senior Member, IEEE

[31] Stark, L. (1974). Microwave Theory of Phased-Array Antennas-A Review. 62(12).

[32] George Oltman. The compensated Balun. IEEE Transactions on Microwave Theory and Techniques (1966). 3(April 1939).

[33] Baumgartner, P., Bauernfeind, T., Biro, O., Hackl, A., Magele, C., Renhart, W., & Torchio, R. (2018). Multi-Objective Optimization of Yagi-Uda Antenna Applying Enhanced Firefly Algorithm with Adaptive Cost Function. IEEE Transactions on Magnetics, 54(3).

[34] Arceo, D., & Balanis, C. A. (2012). Design methodology for a reactively loaded Yagi-Uda antenna. IEEE Antennas and Wireless Propagation Letters, 11(3), 795–798.

[35] Rahim, M. K. A., Aziz, M. Z. A. A., & Goh, C. S. (n.d.). Bow-Tie Micrsotrip antenna Design.

[36] W. Yu, Z. Zhang, A. Zhang and X. Wu, "A broadband dual-polarized magneto-electric dipole antenna for 2G/3G/LTE applications," 2017 Sixth Asia-Pacific Conference on Antennas and Propagation (APCAP), Xi'an, 2017, pp. 1-3.